DOI: 10.1007/s12541-013-0059-1

Springback Nonlinearity of High-strength Titanium Alloy Tube upon Mandrel Bending

Heng Li[1,#], He Yang[1], Fei-Fei Song[1], and Guang-Jun Li[2]

1 State Key Laboratory of Solidification Processing, School of Materials Science, Northwestern Polytechnical University, Xi'an, China, 710072
2 Chengdu Aircraft Industry (Group) Corporation Ltd., Chengdu, China, 610092
Corresponding Author / E-mail: lhseeplan@gmail.com, TEL: +86-29-8849-5632, FAX: +86-29-8849-5632

KEYWORDS: Springback, Tube bending, Nonlinearity, Titanium alloy, High strength

Taking the stress-relieved Ti-3Al-2.5V tube as the objective, regarding both angular and radius springback, the nonlinear springback behaviors of the high-strength titanium tube (HSTT) upon the universal bending, viz., mandrel bending (rotary draw bending), are clarified. The experiments are conducted to identify the springback and validate the theoretical models, and the deformation theory of plasticity and the explicit/implicit 3D-FE based models are used to reveal the rules and the physical mechanism of the nonlinearity of elastic recovery. The results show that: 1) At early bending stages, the angular springback increases nonlinearly with larger bending angles, then it increases linearly when the bending angle exceeds a critical one; While the radius growth decreases exponentially with the increasing of the bending angles at early stages, then it remains unchanged when the bending angle exceeds another critical value; The springback behaves more nonlinearly under smaller bending radii; Both the critical values for the two springback phenomena become larger with smaller bending radii; The critical angle for radius springback is larger than the one for angular springback. 2) The relationship between the radius springback and angular one is further identified; The radius springback can be estimated by the angular springback of the bending regions of tube; The variation of bending radii has significant effect on angular and radius springback, while it has little influence on the springback angle by the straight regions; The variation of the material properties affects both the springback phenomena much more significantly than the changing of the processing parameters.

Manuscript received: October 12, 2012 / Accepted: December 9, 2012

NOMENCLATURE

$\Delta\varphi$ = total springback angle
$\Delta\varphi_b$ = springback angle of the bending portion of tube
$\Delta\varphi_s$ = springback angle of two straight portions of tube
$\Delta\rho$ = radius springback (radius growth)

1. Introduction

High strength titanium alloy bent tube has obtained increasing application as "bleeding" transforming parts in aviation and aerospace industries such as aircraft.[1,2] Due to relatively high efficiency and accuracy with multi-tool constraints (shown in Fig. 1), the mandrel bending (rotary draw bending) is commonly used to realize the bending forming of titanium alloy tubes. However, due to high ratio of yield strength to Young's modulus, the pronounced springback of titanium alloy tube, viz., the decrease of bending angle and increase of bending radius, occurs inevitably after bending, and greatly weakens the forming accuracy and efficiency. Considering the much closer tolerance of production in aerospace industries, the springback should be strictly compensated to ensure the precision bending deformation. Nowadays, regarding springback angle, the knowledge on the linear relation between springback angle and bending angle is commonly adopted to control the springback. While, due to the tri-nonlinear nature of mandrel bending, the above linear relationship cannot work well in many cases, especially for bending with small bending angles. The "trial-error" method is frequently used to compensate for the springback angle by know-how experience and many runs of experiments. Furthermore, due to lacking of knowledge on radius springback, the bending radius growth is not considered, not to saying its compensation. Thus, for achieving the precision bending deformation of titanium alloy tube, both angular springback and radius growth should be considered, and their nonlinear behaviors should also be obtained.

Up to now, great efforts have been conducted on tube bending

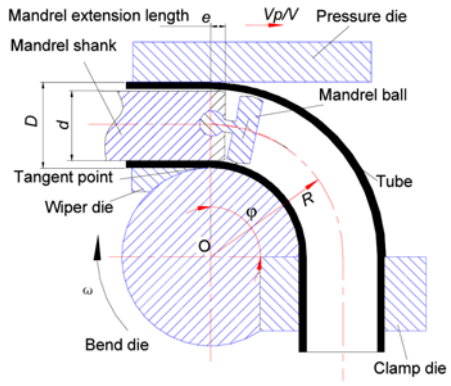

Fig. 1 Principle of tube mandrel bending

regarding wall thinning, cross-section distortion and wrinkling using experimental, analytical or numerical approaches.[3-10] As for the springback in tube bending, most study focused on stainless steel tube or Al-alloy tube.[11-20] The study[11] experimentally confirmed the linear relationship between springback angle and bending angle, while the nonlinear behaviors and physical mechanism of the springback were not addressed as well as the relation between bending angle and radius springback. In the literature,[12] the deformation theory of plasticity was used to deduce the analytical formulae for bending moment and springback calculation. Via the beam bending theory, the authors[13] derived an analytical formula for prediction of tube springback and residual stress distributions in bending with the assumptions of the ideal elastic-plastic material, plane strain condition, the absence of defects and Bauschinger effects. Using the exponential hardening law, the study[14] provided an analytical solution for springback prediction of thin-walled stainless steel tube bending. However, the radius springback was not considered in the above solutions, and the nonlinear behaviors of springback are not addressed. It is noted that, though many factors cannot be considered such as the contact conditions and unequal stress/strain distributions, the analytical models can provide insight into the physical mechanisms of the spirngback phenomenon.

By using the FE method, the study[15] explored the strain hardening effect on springback of Al-alloy and stainless steel tubes in both draw-bending and press bending. The literature[16] proposed a numerical-analytical method to predict the springback angle of thin-walled tube upon mandrel bending, while the stress/strain states of bent-tube were calculated by rigid-plastic FE simulation. Based on the simulation of the whole process including tube bending, mandrel retracting and unloading,[17] the study found that the springback angle considering mandrel retracting was much smaller than that not considering mandrel retracting. By using the 3D-FE models, the study[18] investigated the geometry-dependent springback of 6061-T4 Al-alloy tube upon mandrel bending. Recently, the numerical study[19] was conducted on the coupling effects of the material properties on the springback angle for middle strength Ti-3Al-2.5V tube bending of 14×1.35 mm (outer diameter $D \times$ wall thickness t). The authors[20] clarified the significant springback of high strength Ti-3Al-2.5V tube compared with those of 5052O and steel tube upon mandrel bending. The above methods and results help for the realization of precision tube bending of the high strength titanium alloy tube (HSTT). However, most studies focused on the linear angular springback, and the knowledge on the nonlinearity of both springback angle and radius springback were not mentioned.

Table 1 Friction conditions in various contact interfaces

	Contact interfaces	Tool materials	Coefficients of friction (CoF)
1	Tube outside-wiper die	Al-bronze	0.1
2	Tube outside-pressure die	Cr18MoV	0.25, 0.275, 0.3, 0.325, 0.35
3	Tube outside-clamp die	Cr18MoV	Rough
4	Tube outside-bend die	Cr18MoV	0.25
5	Tube inside-mandrel	Al-bronze	0.05, 0.075, 0.1, 0.125, 0.15
6	Tube inside-flexible balls	Al-bronze	0.1

In this study, taking high strength Ti-3Al-2.5V tube as the objective, the nonlinear behaviors of the HSTT springback upon mandrel bending are focused considering variations of both bending angles and bending radii. Combining with the experiments and analytical analysis, many runs of 3D-FE numerical studies are carried out to reveal the nonlinear behaviors of HSTT springback under various conditions, viz., changing of bending angles, bending radii, variations of material properties and processing parameters. The mandrel bending tests are performed to identify the nonlinear springback and validate the theoretical modeling; Both the plasticity deformation theory and the 3D-FE based theoretical models provide thorough insight into the underlying physical mechanism of the springback by considering nonlinear bending deformation in bending.

2. Experimental Procedure

In mandrel bending (shown in Fig. 1), both sides of tube are subjected to multi-tool constraints. By clamp die and pressure die, the tube is clamped against bend die; then clamp die and bend die rotate simultaneously, and the tube is drawn past the tangent point and rotates along the bend die groove to obtain the desired bending angle and radius. Then the mandrel is withdrawn and the tube is unloaded by removing the tools. Thus the whole bending is finished.

Various defects such as wrinkling, over thinning and cross-section distortion should occur with inappropriate tool design and forming conditions. For springback study, to ensure a defect free bending, the wiper die and mandrel die with one flexible balls are added besides the basic tools, viz., bend die, pressure die and clamp die. In addition, the material types for bending tools should be assigned deliberately as shown in Table 1 due to the different role of friction in tube bending.[21] The lubricant is IRMCO GEL 980-301. The electronic servo drive control bending machine, viz., DYNAMO-E LR150 is used as the experimental platform. Table 2 shows the forming parameters for stable bending experiments of 9.53×0.51 mm. In the experiments, the CoFs of tube-pressure die and tube-mandrel are 0.3 and 0.05, respectively. The V_p/V is one, and e is zero.

The material is the stress relieved Ti-3Al-2.5V tube.[2] The uniaxial tension tests are conducted according to the GB/T228-2002, in which a piece of tube specimen was directly cut from the raw tube by the wire cut. By inserting a tube plug, the tube is clamped and tensioned in a 200KN CMT5205 test machine. Both the longitudinal and vertical extensometers are used for accurate strain records. The velocity of the cross-head is 3 mm/min to ensure a quasi-static process. Fig. 2 shows the average true stress-strain curves of the HSTT with different tube sizes. The exponent hardening law as $\sigma = K(\varepsilon_0 + \varepsilon)^n$ is used to

Table 2 Forming parameters in the experiments and the FE models

Items		Values
Specification of HSTT bending R		1.5D, 2.0D, 2.5D, 3.0D
Bending speed [°/s]		66.5
Relative pushing speed Vp/V		0.9, 0.95, 1, 1.05, 1.1
Bending angle [°]		5, 10, 20, 30, 101.3, 120, 166.5
Dimensions of mandrel	Mandrel diameter d [mm]	8.35
	Mandrel extension length e [mm]	0, 0.25, 0.5, 0.75, 1
	Number of balls	1
	Thickness of balls [mm]	3.5
	Pitch of balls [mm]	2.0
	Ball diameter [mm]	8.32
	Length of mandrel shank [mm]	120
Dimensions of other tools	Length of clamp die [mm]	28.6
	Length of pressure die [mm]	132.7
	Length of wiper die [mm]	300

Note: Vp-pushing speed of pressure die, V-bending speed of bend die

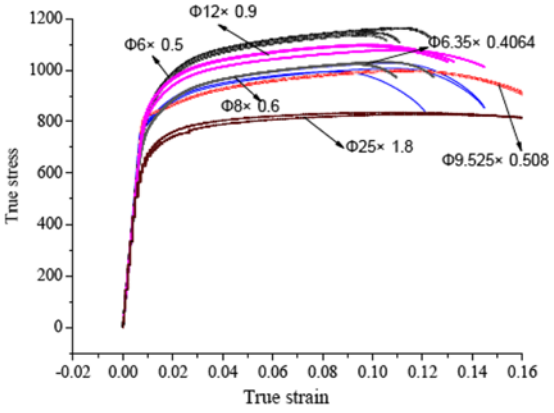

Fig. 2 True stress-strain curves of HSTT with different tube sizes

Table 3 Mechanical properties of different tubular materials

Materials	HSTT	5052-O	1Cr18Ni9Ti
Geometrical specification [$D \times t$]	Φ9.53 × 0.51	Φ50 × 1.5	Φ38 × 1.0
Young's modulus E [GPa]	104.9	55	200
Fracture elongation [%]	18.75	22	60.3
Initial yield stress [MPa]	817.5	90	213
Strength coefficient K [MPa]	1239.55	431	1591
Strain hardening exponent n	0.091	0.262	0.54
Material constant ε_0	0.00035	0	0
Normal anisotropy exponent r	1.508	0.55	0.94
Yield stress/Young's modulus	0.78	0.16	0.11

Table 4 The variations of the material properties for HSTT

Material properties	Value 1	Value 2	Value 3
Young's modulus E [GPa]	88.90	104.86	120.28
Initial yield stress [MPa]	787.5	817.5	847.5
Strength coefficient K [MPa]	1139.55	1239.55	1339.55
Strain hardening exponent n	0.07136	0.0914	0.11136
Normal anisotropy exponent r	1.08	1.51	1. 98

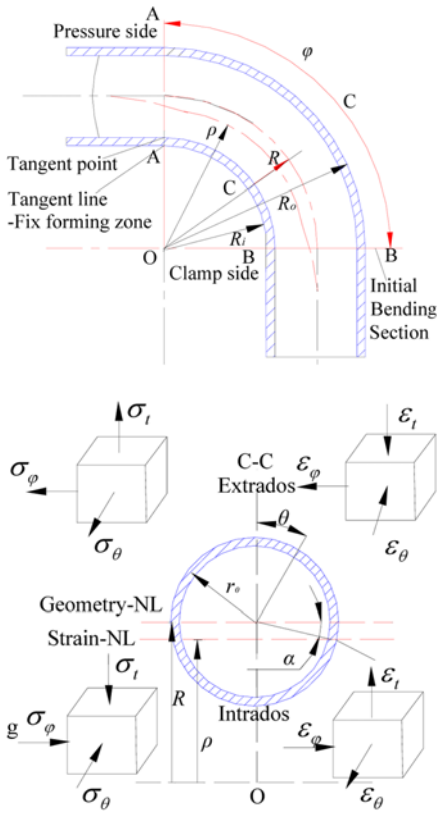

Fig. 3 Geometrical specifications and stress-strain distribution of tube upon mandrel bending

calibrate the stress-strain curves. Table 3 shows the mechanical properties of the Ti-tube with the specification of 9.53 × 0.51 mm. It shows that the HSTT possesses a much higher Yield stress/Young's modulus ratio than the ones of Al-alloy tube and stainless steel tube. Due to complex fabrication processing such as hot extrusion, multi-pass rolling and interval annealing and final stress-reliving, the material properties of the HSTT with different tube sizes or even the same stock present a scattering feature as Table 4.

3. Prediction Models for Tube Springback

3.1 Analytical modeling

The deformation theory of plasticity is used to develop an analytical springback prediction model. The basic assumptions are as follows: The cross-section of the tube remains in a plane during bending; The wall thinning and cross-section deformation are not considered in unloading analysis; The plane strain is regarded; The stress-strain response follows the exponent law as $\sigma = K(\varepsilon_0 + \varepsilon)^n$; The inner side surface of the tube contacts with the groove surface of the bending die in bending (shown in Fig. 3); The stress and strain are uniformly distributed along the bending curves. The length of the fiber of tube before and after unloading is minor.

On release of the external bending loads, the tensile stresses at the extrados of tube and the compressive stresses at the intrados induce a net internal bending moment or residual stresses. The residual stresses cause a decreased change of the bending angle, $\Delta\varphi$, and an increased change of bending radius, $\Delta\rho$. As shown in Fig. 4, the angular springback

in tube bending is induced not only by the plastically deformed bending region of tube, but also by the regions near two straight ends of tube, where the deformation is dominated by the elastic one. Thus, the total springback angle $\Delta\varphi$ of tube should be represented by

$$\Delta\varphi = \Delta\varphi_b + \Delta\varphi_s \tag{1}$$

where $\Delta\varphi_b$ is the springback angle of the curved bending portion of tube, $\Delta\varphi_s$ the springback angle of two straight portions of tube.

Before and after unloading, the length of the tube fiber can be represented

$$\rho\varphi = \rho'\varphi' = (\rho+\Delta\rho)(\varphi-\Delta\varphi_b) \tag{2}$$

The radius springback $\Delta\rho$ and the angular springback by the bending portion $\Delta\varphi_b$ can be deduced as followings.

The bending moment M can be calculated as

$$\begin{aligned} M &= 2\int_0^{D/2} \sigma_\varphi y dA = 2\int_0^{\pi} \sigma_\varphi (r_o\cos\theta)(r_o t d\theta) \\ &= C\int_0^{\pi}\left[\varepsilon_0 + \frac{1+r}{\sqrt{1+2r}}\ln\frac{R+r_0\cos\theta}{\rho}\right]^n \cos\theta d\theta \end{aligned} \tag{3}$$

where $\sigma_\varphi = K\left(\varepsilon_0 + \frac{1+r}{\sqrt{1+2r}}\ln\frac{R+r_0\cos\theta}{\rho}\right)^n / \sqrt{\frac{5}{4}-\frac{r}{1+r}}$, which is the axial stress, $\rho = \sqrt{R_o \times R_i} = D/2\sqrt{2(R/D)^2-1}$, which is the curvature radius of the strain neutral layer (shown in Fig. 3), R_o the outer radius, R_i the inner radius, $C = 2Ktr_o^2/\sqrt{\frac{5}{4}-\frac{r}{1+r}}$.

After the unloading, both the stress change and the stain change can be expressed as

$$\Delta\sigma_\varphi = Mr_0/I \tag{4}$$

$$\Delta\varepsilon_\varphi = \frac{r_0}{\rho} - \frac{r_0}{\rho'} \tag{5}$$

where $I = \pi(D_o^4 - D_i^4)/64$ inertial moment of round tubular materials, D_o and D_i outer and inner diameter of tube, respectively.

It is thought that the elastic strain store energy is totally released without any residual elastic strain. According to the Hooke's law $\Delta\sigma_\varphi = E\Delta\varepsilon_\varphi$ and combining Eq.(4)-(5), the curvature change before and after unloading is

$$\frac{1}{\rho} - \frac{1}{\rho'} = \frac{M}{EI} \tag{6}$$

Thus, the radius ρ' after unloading can be obtained as

$$\rho' = \frac{\rho}{1 - \dfrac{C\int_0^{\pi}\left[\varepsilon_0 + \frac{1+r}{\sqrt{1+2r}}\ln\frac{R+r_0\cos\theta}{\rho}\right]^n \cos\theta d\theta}{EI}\rho} \tag{7}$$

The radius growth $\Delta\rho$ after springback can be obtained

$$\Delta\rho = \frac{\rho}{1 - \dfrac{C\int_0^{\pi}\left[\varepsilon_0 + \frac{1+r}{\sqrt{1+2r}}\ln\frac{R+r_0\cos\theta}{\rho}\right]^n \cos\theta d\theta}{EI}\rho} - \rho \tag{8}$$

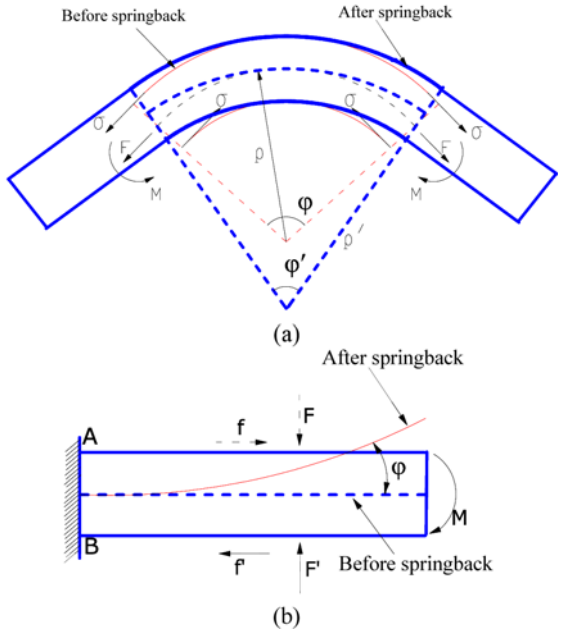

Fig. 4 Mechanical models of the springback of tube bending (a) Bending portion; (b) Straight portion

So by Eq. (2), the change of the bending angle can be obtained

$$\begin{aligned} \Delta\varphi_b &= \left(1-\frac{\rho}{\rho'}\right)\varphi \\ &= \frac{C\int_0^{\pi}\left[\varepsilon_0 + \frac{1+r}{\sqrt{1+2r}}\ln\frac{R+r_0\cos\theta}{\rho}\right]^n \cos\theta d\theta}{EI}\rho\varphi \end{aligned} \tag{9}$$

Thus, via Eq. (8) and Eq. (9), both angular springback $\Delta\varphi_b$ and radius growth $\Delta\rho$ can be numerically calculated to provide intricate insight into the springback mechanism in mandrel bending of HSTT. It is noted that the terms in the curly bracket cannot be explicitly integrated and so its value is numerically approximated by the Trapezoidal numerical integration. It is noted that the proposed analytical model considers both the bending specifications (tube diameter D, wall thickness t, bending radius R) and the material properties (strain hardening exponent n, strength coefficient K and normal anisotropic exponent r). Though the multi-tool constraints and corresponding tensile/compressive stress induced by the pressure die and clamp die cannot considered, the above analytical formulae can provide direct understanding on springback.

3.2 3D-FE modeling of the whole mandrel bending

Over 200 3D-FE models (shown in Fig. 5) of the whole mandrel bending including bending, ball retracting and unloading are established to quantitatively and thoroughly relate the springback with the bending deformation history. The detailed issues involved in FE modeling can be found in the literature.[17,20] The major issues of the modeling are articulated.

The explicit algorithm is used for solving the bending and balls retracting operations; while the implicit one is employed for unloading computation. The stress/strain fields from the bending and ball retracting in explicit simulation are directly imported into standard one for springback calculation. The geometrical nonlinearity is considered

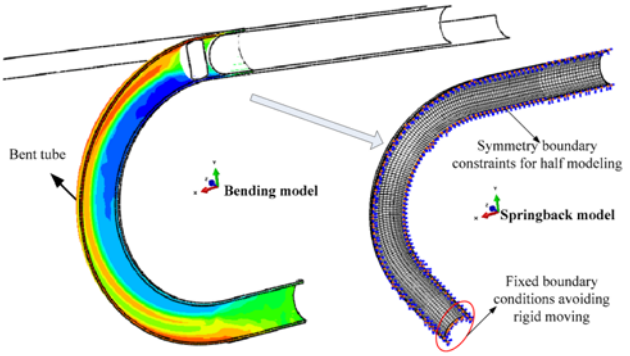

Fig. 5 3D-FE explicit/implicit models for the whole mandrel bending

and the damping factor of 0.002 to stabilize the implicit iteration procedures. In bending simulation, the mass scaling of 5000 is utilized to achieve the tradeoff between computation accuracy and cost by the convergence analysis.

The Hill (1948)'s anisotropic yield function is used to describe the tube's yield behavior; The tube is discretized by a 3D linear reduction integration continuum element with eight nodes and enhanced hourglass control, while a 3D bilinear rigid quadrilateral element is used to model the rigid dies; Different mesh density is applied to different regions of tube with the minimum element size of 3 × 3 mm, and four integration points with Simpson integration rule is used through the tube wall thickness.

The Coulomb friction law $\tau = \mu p$ (τ the frictional shear force, μ the coefficient of friction (CoF), p the pressure force on the contact surface) is used to model the friction behavior. The detailed contact conditions and friction information are summarized in Table 1. For bending process, the boundary constraints are applied by two approaches: "displacement/rotates" and "velocity/angular". As shown in Fig. 5, both the bend die and the clamp die are constrained to simultaneously rotate about the global Z-axis; The pressure die is constrained to translate only along the global X-axis; The wiper die is constrained along all freedom degrees; The mandrel (including mandrel shank and multi-balls) is kept stationary along x-axis during bending, while the mandrel is retracted when the bending deformation is finished; The "connector element" is used to define the "hinge" contact behaviors between mandrel shank and flexible balls. The trapezoidal profile is used to define the smooth loading of all the above tools to reduce inertial effects in the explicit simulation. As shown in Fig. 5, for unloading process, all tools are removed and a fixed boundary condition is applied to avoid the rigid motion.

4. Results and Discussion

4.1 Evaluation of the theoretical models

A series of bending experiments have been conducted with various bending angles from 5° to 166.5° to validate the theoretical models. The forming conditions are shown in Table 2. The wiper die was not used. Fig. 6 shows the HSTT bent parts with bending angles of 5°, 10° and 30°. Since the cross-section distortion occurs mainly on the extrados of tube, as shown in Fig. 7, the curvature change of the inner crestline of tube can thus be used to represent the curvature change before and after

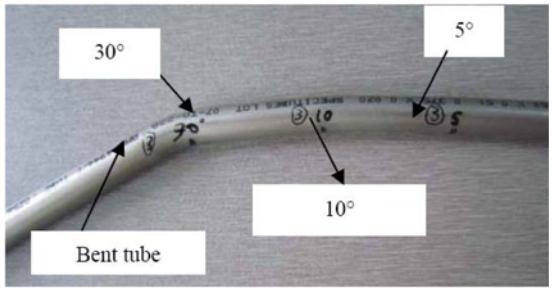

Fig. 6 HSTT bent tubes with small bending angels

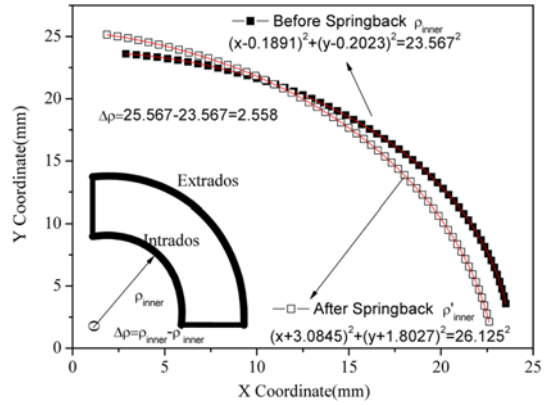

Fig. 7 Intrados of bent tube and its circle fitting before and after springback for 2.5D bending

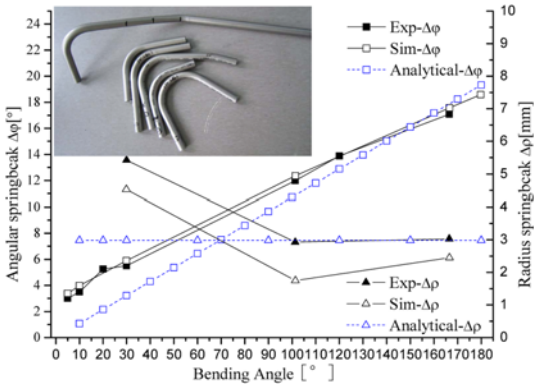

Fig. 8 Springback comparison between the experimental results and the theoretical ones

springback as Eq. (10). While, in the simulation, the curvature can be obtained by the circle function fitting.

$$\Delta\rho = \rho' - \rho = \rho'_{inner} - \rho_{inner} \tag{10}$$

As shown in Fig. 8, it is confirmed that there occurs significant springback for HSTT in tube bending. The FE numerical prediction provides consistent tendency of the elastic recovery with bending angles, viz., at early bending stages, both the angular springback $\Delta\varphi$ and radius springback $\Delta\rho$ behave nonlinearly; while at later stages, the $\Delta\varphi$ increases linearly with the larger bending angles, and the $\Delta\rho$ changes little. The FE numerical predictions for $\Delta\varphi$ and $\Delta\rho$ agree with the experimental ones with the relative error less than nearly 10% and 35%, respectively. The discrepancy is mainly caused by two reasons, viz., 1) the idealized contact conditions are used in FE modeling such

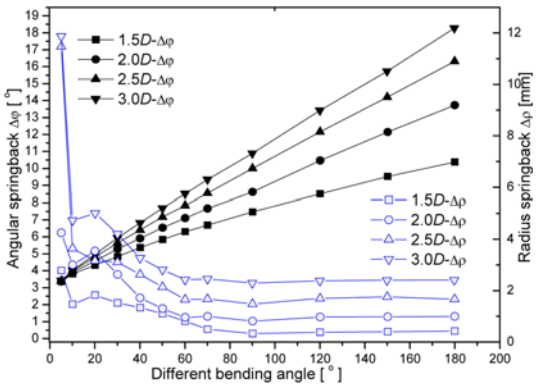

Fig. 9 Angular and radius springback of HSTT under different bending radii and bending angles

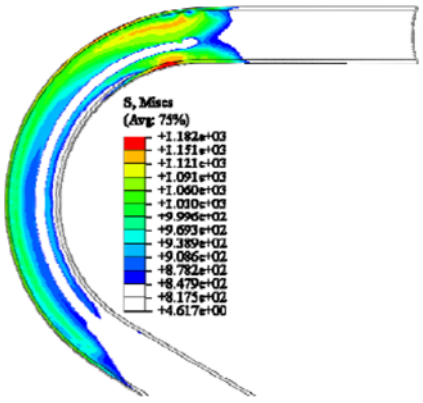

Fig. 10 Mises stress (MPa) distributions in mandrel bending of 3.0*D*

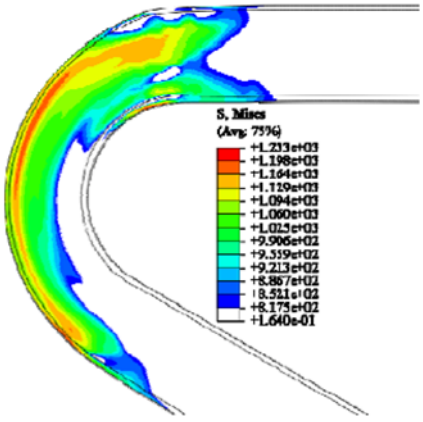

Fig. 11 Mises stress (MPa) distributions in mandrel bending of 1.5*D*

as the stable friction conditions and the tooling movements; 2) the mechanical properties of the HSTT is not fully captured by the current constitutive relationship such as the possible variation of the Young's modulus *E*. The prediction error for $\Delta\rho$ is larger than that for $\Delta\varphi$ due to larger measure error of the radius growth. However, it is noted that the discrepancy between analytical predictions and experimental ones is much larger than that between FE numerical results and experimental ones. This discrepancy even becomes much obvious at early bending stage. This deviation is mainly caused by the assumptions stated in the Section 3.1. In analytical formulae, the homogeneous stress/strain distributions are calculated. Thus, the nonlinear behaviors of springback cannot be represented by the analytical ones, and the FE numerical one possesses this capability. In the following sections, the nonlinearity of the springback is deeply analyzed.

4.2 Springback nonlinearity of HSTT under different bending radii and bending angles

Under different bending radii of 1.5*D*, 2.0*D*, 2.5*D* and 3.0*D* (1.5*D* means 1.5 times outer diameter of tube diameter *D*), the nonlinearity of the HSTT springback is explored by changing different bending angles. Fig. 9 shows that both the angular springback $\Delta\varphi$ and radius springback $\Delta\rho$ become larger with the increases of the bending radii, which is attributed to the larger elastic strain energy stored under larger bending radii. Fig. 10 and Fig. 11 show the Mises stress distributions of 150° tube under *R* of 3.0*D* and 1.5*D*, respectively. The colorful contour refers to the region where the plastic deformation happens. We observed that, for large bending radius of 3.0*D*, there exists significant elastic deformation bands near the geometrical neutral layer of tube, thus larger elastic strain energy is accumulated. While for bending with smaller bending radius of 1.5*D*, the more severe bending deformation is induced and the fully plastic deformation occurs cross the whole cross-section of tube, which causes less accumulation of the elastic strain energy.

For each bending radius, it is noted that, the significant nonlinear behaviors of the springback occur with the increases of the bending angles. Fig. 12 shows the detailed nonlinear information for each bending radius. It is found that the radius springback $\Delta\rho$ decreases sharply at early bending stages, then it decreases gradually with the increase of the bending angles, finally it remains unchanged when the bending angle exceeds one critical value. The critical value of the bending angle is about 60° for bending radii of 3.0*D*, 2.5*D* and 2.0*D*, while the critical one for bending radius of 1.5*D* is about 90°. For the angular springback $\Delta\varphi$, it is found that, at early bending stages, the $\Delta\varphi$ increases nonlinearly with the larger bending angles, and then it increases linearly along the bending process when the bending angle exceeds another critical bending angle. While, it is observed that, this tendency becomes much more nonlinear at later bending stages, and the critical value increases with the decreasing of the bending radii. Especially, there occur totally nonlinear behaviors for all bending angles under bending radius of 1.5*D* as shown in Fig. 12(d).

Generally, as shown in Fig. 12, the tendency of angular springback $\Delta\varphi$ can generally be fitted as a linear function. And the tendency of radius springback $\Delta\rho$ can be fitted as a piecewise function, viz., exponent function at early bending stages and constant function at larger bending stages. However, the deviation between the fitting curves and the numerical predictions becomes larger under smaller bending radii, especially at early bending stages. However, as shown in Fig. 9 and Fig. 12, the analytical prediction cannot capture these nonlinear behaviors. According to Eq. (8), the radius springback $\Delta\rho$ is a constant with the larger bending angles for given tubular material and geometrical parameters; According to Eq. (9), for angular springback $\Delta\varphi$, the conventional linear relationship between springback radius and bending angles is established. Why the analytical formulae cannot be used to represent the nonlinear behaviors of HSTT springback. The reason is that the unequal bending deformation occurs at both extrados and intrados of bent tube, which is much difficult to be considered in the analytical modeling.

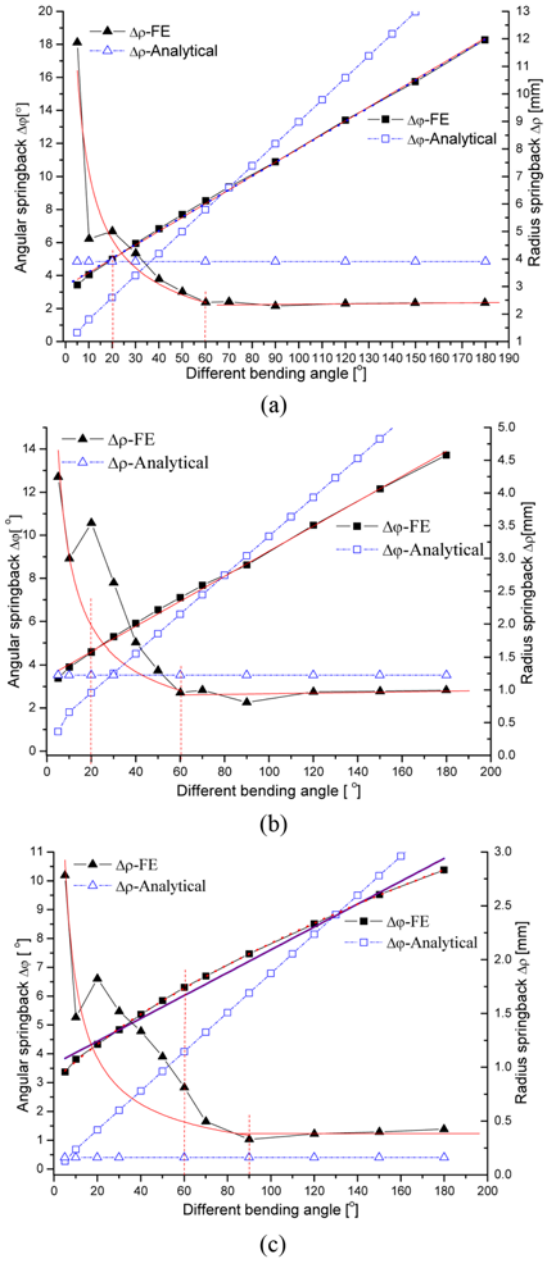

Fig. 12 Springback behaviors of HSTT under different bending radii (red solid line represents the fitting curve of the numerical prediction) (a) 3.0*D* (b) 2.0*D*; (c) 1.5*D*

As shown in Fig. 10, 11, along bending process, the unequal tensile and compressive stress distributions are induced, and there occurs remarkable unequal tensile and compressive plastic deformation at the extrados and intrados of tube, respectively. This unequal states of the stress and strain distributions become more serious under smaller bending radii. For bending with the bending radius of 3.0*D* (shown in Fig. 10), considering both the area and the magnitude, the plastic deformation reaches stable state with Mises stress of about 1186 MPa at bending angle larger than 60°. While, for bending with the bending radius of 1.5*D* (shown in Fig. 11), the plastic deformation behaves unsteadily all most over the whole bending process. That is the reasons why the nonlinear behaviors of the HSTT springback occurs at early bending stages under larger bending radii, while the nonlinearity happens over the whole bending process under smaller bending radii. Thus, the analytical formulae can only be used to represent the general linear tendency at later bending stages under large *R*, and it cannot work well for the springback prediction under smaller bending radii or with the smaller bending angles.

4.3 Relationship between radius springback and angular springback

The relationship between angular springback $\Delta\varphi$ and radius springback $\Delta\rho$ is identified furthermore based on the above nonlinearity analysis of the HSTT springback in mandrel bending. As shown in Fig. 9 and Fig. 12, it is found that the nonlinear behaviors of the $\Delta\rho$ and the $\Delta\varphi$ are different from each other over the bending process, viz., the general contrary tendency with the increase of bending angles, and the different values of the critical bending angle as stated in Section 4.2. For the first difference, it can be explained by Eq. (2), in which an approximately inverse relationship between the $\Delta\rho$ and the $\Delta\varphi$ exists. It is noted that, according to Eq. (2), if the $\Delta\varphi$ linearly increases with the larger bending angle, then the $\Delta\rho$ certainly keeps unchanged. As to the second difference, it is found that the critical angle for the radius springback $\Delta\rho$ is larger than the one for angular springback $\Delta\varphi$. Under the bending radius of 2.0*D*, 2.5*D* and 3.0*D*, the critical value is 60° and 20° for $\Delta\rho$ and $\Delta\varphi$, respectively. And under the bending radius of 1.5*D*, the critical value for $\Delta\rho$ and $\Delta\varphi$ is 90° and 60°, respectively. The second difference should be attributed to the occurring mechanism of the $\Delta\rho$ and $\Delta\varphi$ during unloading of the bent tube mentioned in Section 4.2.

As demonstrated as Eq. (1), the total angular springback $\Delta\varphi$ of tube is composed of two parts, viz., the springback angle $\Delta\varphi_b$ by the curved bending portion and the springback angle $\Delta\varphi_s$ by two straight portions of tube. In the simulation, the $\Delta\varphi_s$ can be calculated by $\Delta\varphi_s = \Delta\varphi - \Delta\varphi_b$ as shown in Fig. 13. The decomposed values of the total springback angle under various bending radii are presented in Fig. 14. It is found that the angular springback $\Delta\varphi_s$ by the two straight ends of tube changes little with the increasing of the bending angles. Upon bending, the plastic deformation extends to the two straight ends of tube, which causes the occurring of $\Delta\varphi_s$, and the deformation regions of the straight ends remains unchanged in bending, thus making the $\Delta\varphi_s$ independent of bending angles. Also, the values of the $\Delta\varphi_s$ are independent of the bending radius. While, the angular springback $\Delta\varphi_b$ by the bending portion passes through the original point and increases linearly with the larger bending angles. The $\Delta\varphi_b$ plays major role in nonlinear effects of the total angular springback $\Delta\varphi$. That is why the linearly fitted Eq. (11) can well represent the angular springback tendency in many cases. The fixed ratio is thought to represent the springback amount by the straight regions of tube, and the proportional ratio represents the linear slope between springback angle and bending angles. Since the analytical model in Section 3.1 considers only the bending curved region, the fitting curve of the corresponding prediction passes through the origin point as shown in Fig. 9. It is thought that the initial unequal deformation upon bending makes the proportional constant vary with the increasing of the bending angles, which dominates the nonlinear mechanism of the angular springback $\Delta\varphi$. However, the radius springback $\Delta\rho$ is induced mainly by the unequal deformation of the curved bending portion. Thus, the critical value for $\Delta\rho$ is larger than the one for the $\Delta\varphi$.

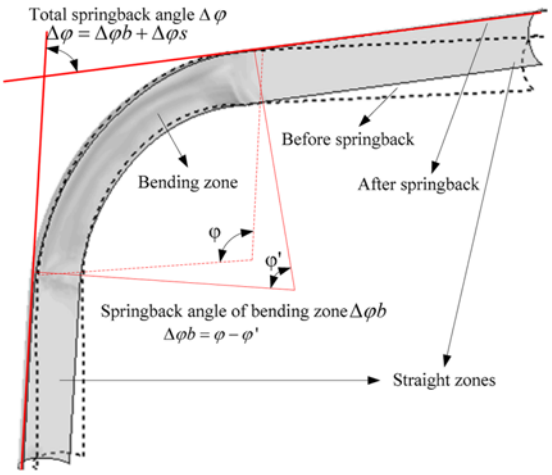

Fig. 13 Measurement schematic of springback

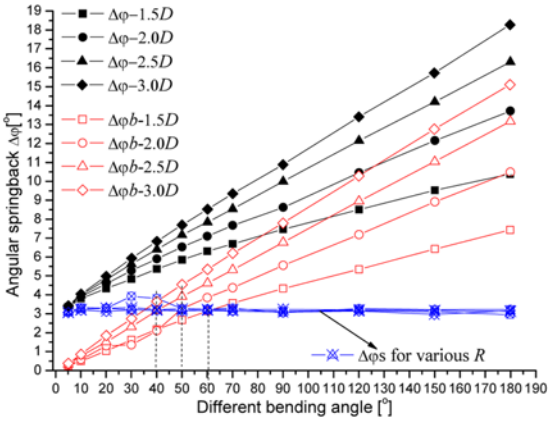

Fig. 14 Springback angle for bending zone and straight zones

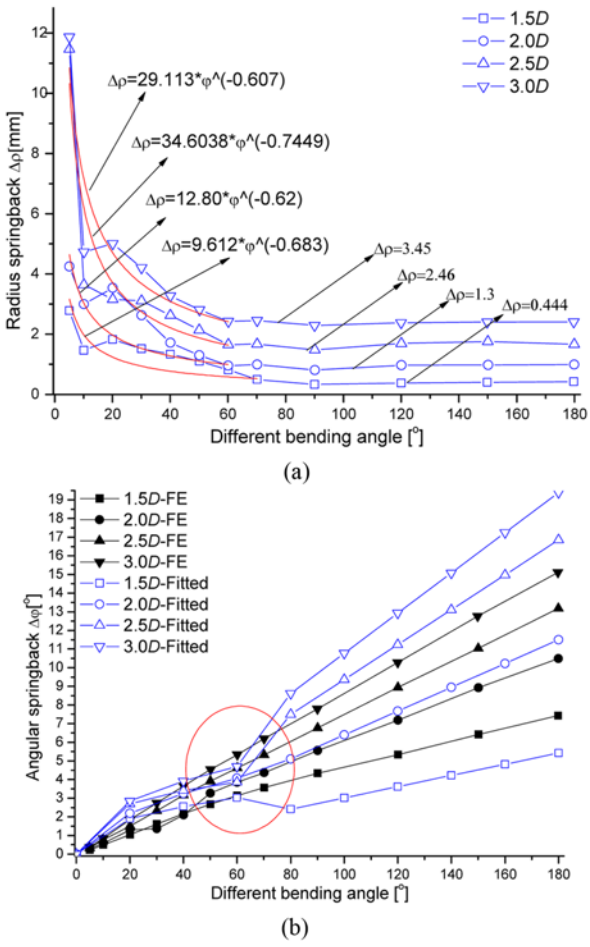

Fig. 15 Nonlinear springback representation of HSTT (a) Radius springback; (b) Angular springback

$$\Delta\varphi = k\varphi + b \tag{11}$$

where k is the proportional ratio, b the fixed ratio.

As shown in Fig. 15, a piecewise function as Eq. (12) can be used to represent the nonlinear behaviors of the radius springback $\Delta\rho$. It is found that, under the smaller bending radius, the fitting error becomes larger due to much more significant nonlinear effects of the radius springback $\Delta\rho$. By using Eq. (2), the angular springback $\Delta\varphi$ along the bending angles is also deduced as Eq. (13). It is noted that, though the general tendency can be represented, the obvious discrepancy happens for bending stages with the bending angles near the critical value.

$$\Delta\rho = \begin{cases} a\varphi^b & \varphi \le \varphi_c \\ c & \varphi > \varphi_c \end{cases} \tag{12}$$

where a, b and c are constants, φ_c the critical bending angle,

$$\Delta\varphi = \begin{cases} (1-\rho/\rho + a\varphi^b)\varphi & \varphi \le \varphi_c \\ c/\rho + c & \varphi > \varphi_c \end{cases} \tag{13}$$

4.4 Springback nonlinear behaviors under variations of material properties and processing parameters

As stated in Section 2, there occurs significant scattering of the material properties of HSTT (shown in Table 4) due to its complex thermo-mechanical fabrication processes.[2] Considering the remarkable effects of the material properties on springback, the nonlinear characteristics of the HSTT under variations of the material properties are thus discussed. The bending radius is 2.0D. Fig. 16 shows, under the same bending conditions, both the $\Delta\rho$ and the $\Delta\varphi$ of the HSTT are far larger than the ones of the stainless steel tube and the Al-alloy tube. While, the similar nonlinear tendencies of both the $\Delta\rho$ and the $\Delta\varphi$ are observed for three tubular materials. It shows that the value of the initial yield stress has little effect on the springback along the bending process, while, Fig. 17 shows that both the strength coefficient K and the Young's modulus E have significant influence on both the $\Delta\rho$ and the $\Delta\varphi$. It is found that the angular springback $\Delta\varphi_s$ of the straight portions is affected greatly by the K and the E, which is different from the effects of the bending radii on springback as shown in Fig. 14. The reason is that, the larger K makes the deformation region extend from the curved bending region to straight ends of the tube, and the smaller E causes the larger elastic energy store capacity, which both help increase the springback of the HSTT. Relatively, the effect significance of the Young's modulus E is slightly greater than the one of the strength coefficient K.

Considering the multi-tool constrained features of the mandrel bending, the nonlinear springback behaviors of the HSTT under variations of the major processing parameters are also addressed. Three processing parameters (including the mandrel extension length e, CoF of tube-mandrel and relative push assistant speed Vp/V) are considered.

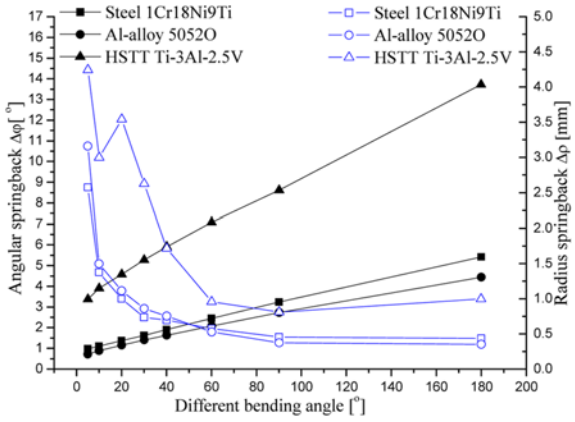

Fig. 16 Comparison of HSTT springback with ones for other materials

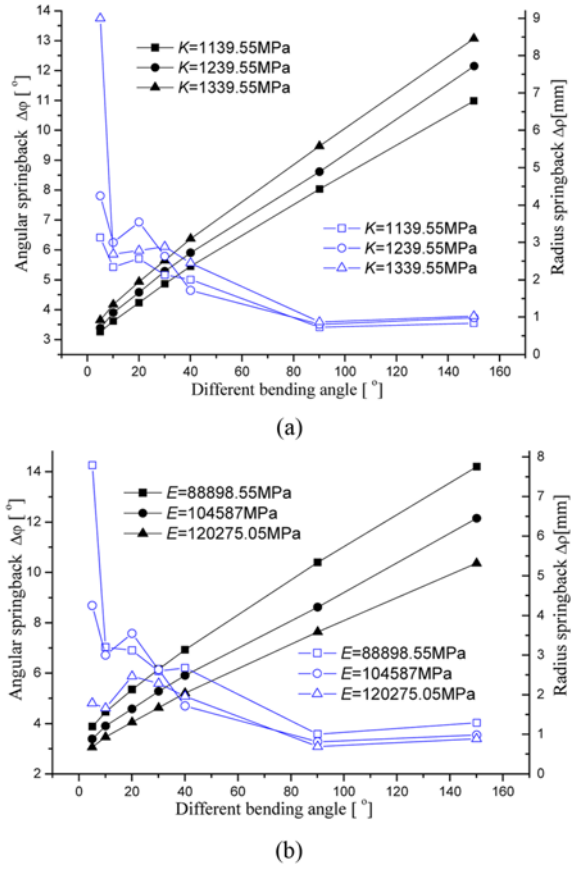

Fig. 17 Springback variations under different tube properties for 2.0D bending (a) *K*; (b) *E*

The variations of the processing parameters are shown in Table 1 and Table 2. It is found that both the mandrel extension length *e* and the CoF of tube-mandrel have little effect on the nonlinear springback behaviors under given scatted parameters, while Fig. 18 shows that the relative pushing assistant speed *Vp/V* has greater effect on both the elastic recovery characteristics. Generally, both the angular springback $\Delta\varphi$ and the radius springback $\Delta\rho$ increase with the larger relative pushing assistant speed *Vp/V*. While, it is found that both the springback phenomena change little with *Vp/V* of 1.0 and 1.1. Also, it is observed that the above three process parameters have little effect on the angular springback $\Delta\varphi_s$ of the straight portions of the bending tube. It is obvious that the nonlinear behaviors of the elastic recovery induced by the changing of the processing parameters are far less significant than the ones caused by bending radius and the material properties.

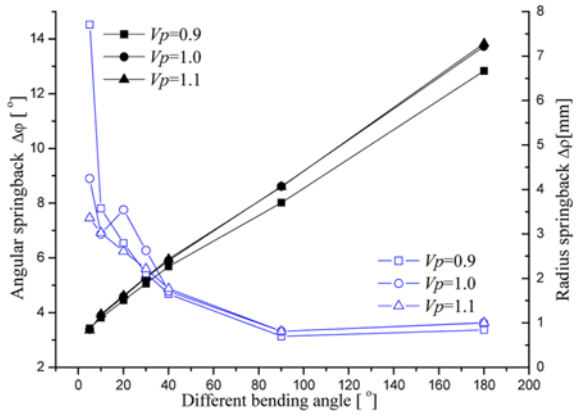

Fig. 18 Springback variation under different *Vp*

5. Conclusions

(1) There occur obvious and unique springback nonlinear behaviors of HSTT in mandrel bending. The nonlinear behaviors of the radius springback $\Delta\rho$ and the angular springback $\Delta\varphi$ are different from each other over the bending process, viz., the general contrary tendency with the increase of bending angles, and the different values of the critical bending angle; The nonlinear springback behaves more obviously with smaller bending radii; Both the critical values for the two springback phenomena increase under smaller bending radii; The nonlinear behaviors of HSTT springback are attributed to the unequal bending deformation and the occurring mechanism of $\Delta\varphi_b$ and $\Delta\varphi_s$.

(2) The relationship between the radius springback and angular one is quantitatively identified and clarified. The angular springback is the sum of the springback by the bending regions and the one by the straight regions of tube; The radius springback can be approximately estimated by the springback angle of the bending regions of tube; The variation of bending radii has significant effect on angular and radius springback, while it has little influence on the angular springback $\Delta\varphi_s$ by the straight regions.

(3) The variations of the tube properties affect both the springback phenomena more significantly than the changing of the processing parameters; Both the Young's modulus and the strength coefficient have larger effects on the springback; Based on the mechanism of the remarkable nonlinear springback, two piecewise models are used to represent the nonlinear behaviors of the HSTT in mandrel bending.

ACKNOWLEDGEMENT

The authors would like to thank the National Natural Science Foundation of China (50905144, 51275415), the Program for New Century Excellent Talents in University, the fund of State Key Laboratory of Solidification Processing, Natural Science Basic Research Plan in Shaanxi Province (2011JQ6004) and the 111 Project (B08040) for the support given to this research.

REFERENCES

1. Boyer, R. R., "An Overview on the Use of Titanium in the Aerospace Industry," Mater. Sci. Eng. A., Vol. 213, pp. 103-114, 1996.
2. SAE Standards, Product Code. AMS4956, "Titanium Alloy Tubing, Seamless, Hydraulic 3Al-2.5V, Textured Controlled Cold Worked, Stress Relieved," 2010.
3. Paulsen, F. and Welo, T., "Application of Numerical-simulation in the Bending of Aluminum-alloy Profiles," J. Mater. Process. Technol., Vol. 58, pp. 274-285, 1996.
4. Oliveira, D. A., Worswick, M. J., Khodayari, G., and Gholipour, J., "Effect of Bending Variables on the Characteristics of En-aw5018 Tubes for Subsequent Hydroforming," Canadian Metallurgical Quarterly, Vol. 46, pp. 145-153, 2007.
5. Trana, K., "Finite Element Simulation of the Tube Hydroforming Process-Bending, Preforming and Hydroforming," J. Mater. Process. Technol., Vol. 127, pp. 401-408, 2002.
6. Yang, J., Jeon, B., and Oh, S., "The Tube Bending Technology of a Hydroforming Process for an Automotive Part," J. Mater. Process. Technol., Vol. 111, pp. 175-181, 2001.
7. Dwyer, N., Worswick, M. J., Gholipour, J., Xia, C., and Khodayari, G., "Pre-bending and Subsequen Hydroforming of Tube: Simulation and Experiment," Porc. of Numisheet 2002 Conference, pp. 447-452, 2002.
8. Gao, L. and Strano, M., "FEM Analysis of Tube Pre-bending and Hydroforming," J. Mater. Process. Technol., Vol. 151, pp. 294-297, 2004.
9. Bardelcik, A., "Effect of Pre-bending and Hydroforming Parameters on the Formability of Advanced High Strength Steel Tube," Ph. D. Thesis, Dept. Mech. Eng., University of Waterloo, 2006.
10. Jeong, H. S., Jeon, J. W., Ha, M. Y., and Cho, J. R., "Finite Element Analysis for Inconel 625 Fine Tube Bending to Predict Deformation Characteristics," Int. J. Precis. Eng. Manuf., Vol. 13, No. 8, pp. 1395-1401, 2012.
11. Lou, H. and Stelson, K. A., "Three-dimensional Tube Geometry Control for Rotary Draw Tube Bending, Part 1: Bend Angle and Overall Tube Geometry Control," J. Manuf. Sci. Eng. ASME, Vol. 123, pp. 258-265, 2001.
12. Tang, N. C., "Plastic-deformation Analysis in Tube Bending," Int. J. Pressure. Vessels Piping, Vol. 77, pp. 751-759, 2000.
13. Al-Qureshi, H. A. and Russo, A., "Spring H.A.-back and Residual Stresses in Bending of Thin-walled Aluminium Tubes," Mater. Design, Vol. 23, pp. 217-222, 2002.
14. E, D. X. and Chen, M., "Numerical Solution of Thin-walled Tube Bending Springback with Exponential Hardening Law," Steel Res. Int., Vol. 84, pp. 286-291, 2010.
15. Murata, M., Kuboki, T., Takahashi, K., Goodarzi, M., and Jin, Y., "Effect of Hardening Exponent on Tube Bending," J. Mater. Process. Technol., Vol. 201, pp. 189-192, 2008.
16. Zhan, M., Yang, H., Huang, L., and Gu, R. J., "Springback Analysis of Numerical Control Bending of Thin-walled Tube Using Numerical-analytic Method," J. Mater. Process. Technol., Vol. 177, pp. 197-201, 2006.
17. Gu, R. J., Yang, H., Zhan, M., Li, H., and Li, H. W., "Research on the Springback of Thin-walled Tube NC Bending based on the Numerical Simulation of the Whole Process," Comput. Mater. Sci., Vol. 42, pp. 537-549, 2008.
18. Li, H., Yang, H., Tian, Y. L., Li, G. J., and Wang, Z. H., "Geometry-dependent Springback Behaviors of Thin-walled Tube upon Cold Bending," Sci. China Tech. Sci., Vol. 55, pp. 1-14, 2012.
19. Jiang, Z. Q., Yang, H., Zhan, M., Xu, X. D., and Li, G. J., "Coupling Effects of Material Properties and the Bending Angle on the Springback Angle of a Titanium Alloy Tube during Numerically Controlled Bending," Mater. Design, Vol. 31, pp. 2001-2010, 2010.
20. Li, H., Yang, H., Song, F. F., Zhan, M., and Li, G. J., "Springback Characterization and Behaviors of High-strength Ti-3Al-2.5V Tube in Cold Rotary Draw Bending," J. Mater. Process. Technol., Vol. 212, pp. 1973-1987, 2012.
21. Yang, H., Li, H., and Zhan, M., "Friction Role in Bending Behaviors of Thin-walled Tube in Rotary-draw-bending under Small Bending Radii," J. Mater. Process. Technol., Vol. 210, pp. 2273-2284, 2011.